Extent of Voltage Sensor Movement during Gating of Shaker K^{+} Channels

David J. Posson[1,2] and Paul R. Selvin[1,*]
[1]Department of Physics and Biophysics, University of Illinois Urbana-Champaign, Urbana IL, 61801, USA
[2]Present address: Department of Anesthesiology, Weill Cornell Medical College, New York, NY 10065, USA
*Correspondence: selvin@uiuc.edu
DOI 10.1016/j.neuron.2008.05.006

SUMMARY

Voltage-driven activation of Kv channels results from conformational changes of four voltage sensor domains (VSDs) that surround the K^{+} selective pore domain. How the VSD helices rearrange during gating is an area of active research. Luminescence resonance energy transfer (LRET) is a powerful spectroscopic ruler uniquely suitable for addressing the conformational trajectory of these helices. Using a geometric analysis of numerous LRET measurements, we were able to estimate LRET probe positions relative to existing structural models. The experimental movement of helix S4 does not support a large 15–20 Å transmembrane "paddle-type" movement or a near-zero Å vertical "transporter-type" model. Rather, our measurements demonstrate a moderate S4 displacement of 10 ± 5 Å, with a vertical component of 5 ± 2 Å. The S3 segment moves 2 ± 1 Å in the opposite direction and is therefore not moving as an S3–S4 rigid body.

INTRODUCTION

Voltage-gated ion channels underlie the propagation of action potentials in the nervous system and are fundamental to cell excitability (Hille, 2001; Hodgkin and Huxley, 1952). The classical Shaker K^{+} channel from *Drosophila* (Tempel et al., 1987) is a widely studied example of the extensive voltage-gated potassium (Kv) channel family. These homotetrameric channels have six transmembrane segments per subunit (S1–S6) that are divided into two distinct modular domains: S1–S4 and S5–S6. (Kumanovics et al., 2002; Murata et al., 2005; Sasaki et al., 2006). The pore domain (S5–S6) forms the permeation pathway, including the K^{+} selectivity filter and channel gates. The S1–S4 segments form the voltage-sensing domains (VSDs) and are peripheral to the pore domain. The VSDs transduce changes in transmembrane voltage into opening or closing of the pore. In Shaker, the S4 segment has six positive charges, of which the first four are arginines responsible for most of the gating charge that moves across the membrane electric field during channel gating (Aggarwal and MacKinnon, 1996; Seoh et al., 1996). Therefore, the movement of S4 is of special significance.

Crystallographic studies have provided a significant amount of static structural detail for the archaebacterial channel KvAP (Jiang et al., 2003a; Lee et al., 2005), a mammalian channel Kv1.2 (Long et al., 2005), and a Kv1.2/2.1 chimera (Long et al., 2007). All of these structures are open/inactivated channels. To date, a structure of a closed Kv channel with inwardly facing gating charges has not been solved. Therefore, the conformational changes within the VSD are still uncertain and require biophysical investigation.

The KvAP crystal structures suggested the possibility of a voltage-sensing S3–S4 structure that moved as a unit 15–20 Å at the protein-lipid interface (Jiang et al., 2003b). This "paddle model" was in sharp contrast with competing models that invoked aqueous crevices within the VSD that focus the membrane electric field over a short gating pathway for S4 arginines (Ahern and Horn, 2004; Bezanilla, 2005; Tombola et al., 2006). These models allow much smaller movements of S4 to account for the 12–14 e_0 of gating charge (Ahern and Horn, 2005; Chanda et al., 2005; Starace and Bezanilla, 2004).

Fluorescence studies of voltage-gated channels have relied heavily on voltage-driven environmental changes recorded as emission intensity differences (Blunck et al., 2004; Cha and Bezanilla, 1997; Chanda et al., 2004; Gandhi et al., 2003; Mannuzzu et al., 1996; Pathak et al., 2005; Smith and Yellen, 2002; Sonnleitner et al., 2002). These studies are able to detect and track conformational changes but remain silent on the specific magnitude and manner of protein movement. More quantitative studies have used fluorescence resonance energy transfer (FRET) (Glauner et al., 1999) and LRET (Cha et al., 1999; Posson et al., 2005; Richardson et al., 2006) as spectroscopic rulers, determining the distance between donor and acceptor probes within the protein (Clegg, 1995; Selvin, 2002; Stryer and Haugland, 1967). LRET in particular is an approach that is uniquely suited for estimating structural distances on the Shaker channel within cell membranes and can be used to study open and closed conformational states of the channel. Using LRET between VSD sites and a pore-blocking charybdotoxin (CTX), we previously estimated the degree of S4 movement to be only 2 Å normal to the membrane (Posson et al., 2005). These measurements ruled out the large movements required by the paddle model in support of a highly focused electric field model but did not further elucidate the mechanism underlying voltage sensing. We have now filled this gap with a thorough exploration of LRET measurements across 19 sites on or just external to S1–S4, which has allowed us to estimate movements of VSD helices in three dimensions. We find the motion of S4 to be the most significant change within the VSD during gating. Our measurements indicate an S4 displacement on the order of 10 Å with a vertical
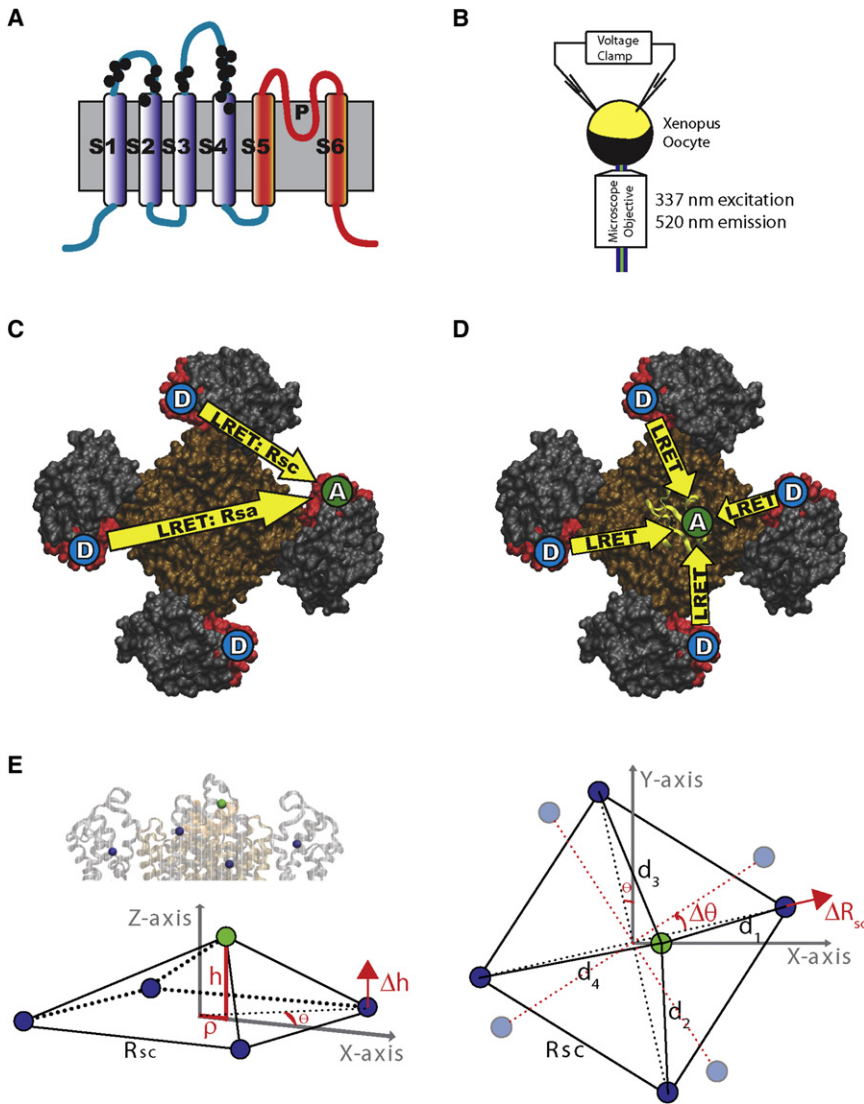
Figure 1. Experimental Design

(A) Topology of a single subunit of the Shaker K^+ channel. The gray background represents the membrane, the voltage-sensing domain (S1–S4) is blue, and the pore domain (S5–S6) is red. Black dots indicate sites that were mutated to cysteine and used in LRET experiments.

(B) Whole oocytes were clamped using a two-electrode voltage clamp mounted on an inverted microscope. Excitation pulses (337 nm) from a N_2 laser were directed onto the oocyte, and fluorescence was collected with photomultiplier tube detectors.

(C) Location of donor and acceptor probes for VSD to VSD LRET experiments illustrated using the Kv1.2 chimera structure (Long et al., 2007) viewed from above. Distances measured are Rsc (subunit contiguous) and Rsa (subunit across). The S4 segment is colored red for emphasis.

(D) Location of donor and acceptor probes for VSD to CTX LRET experiments. The CTX peptide is a yellow ribbon. Four distances (d_1, d_2, d_3, and d_4) are measured.

(E) Square, oblique pyramid model used to interpret LRET results. Geometric parameters ρ, h, and θ are calculated from the measured LRET distances indicated. Probe coordinates (x, y, z) are calculated using the coordinate system shown. VSD conformational changes (red arrows) are expressed as changes in h (vertical movement), θ (tangential movement), and Rsc (radial movement).

component of 5 ± 2 Å, significantly greater than the previous estimate from LRET. A change of this magnitude better explains the large gating charge movement even across a highly focused electric field and is consistent with recent structural models (Campos et al., 2007; Pathak et al., 2007). Such a movement remains in contrast to the paddle model as originally proposed (Jiang et al., 2003b) or as recently modified by MacKinnon and coworkers (Long et al., 2007).

RESULTS

LRET-Derived Distances on the Shaker K^+ Channel

LRET is a spectroscopic ruler capable of measuring the distance between a lanthanide donor probe, Tb-DTPA-cs124-EMPH (Chen and Selvin, 1999), and a fluorescent acceptor molecule. LRET improvements over conventional FRET result from the long lifetime and narrow spectrum of the Tb^{3+} donor, allowing detection of acceptor fluorescence due only to energy transfer (Selvin, 2002). Distances can easily be measured in the presence

of donor-only and acceptor-only populations, including the large instantaneous autofluorescence, making LRET on *Xenopus* oocyte membranes possible. In addition, the zero intrinsic anisotropy of Tb^{3+} insures that energy transfer measurements are only related to the distance between donor and acceptor, not to the relative orientation of the dyes (Reifenberger et al., 2003). Externally accessible protein sites on or just external to S1–S4 (black dots, Figure 1A) are individually mutated to cysteine to which thiol-reactive probes are then specifically attached. Shaker channels are expressed in *Xenopus* oocytes and controlled with a whole-oocyte two-electrode voltage clamp mounted on an inverted fluorescence microscope for collection of LRET data (Figure 1B).

Previous LRET experiments on Shaker have used two complementary approaches for measuring conformational changes. The first (Cha et al., 1999) measures the VSD to VSD distance between contiguous subunits (Rsc) and across the channel (Rsa) (Figure 1C). This experimental arrangement is most sensitive to protein movement radial to the channel symmetry axis (Figure 1E, ΔRsc). The second approach (Posson et al., 2005) measures distances between lanthanide donor-labeled VSD sites and an acceptor-labeled pore-blocking toxin, charybdotoxin (CTX) (Figure 1D). This arrangement is more sensitive to movement in the vertical direction (normal to the membrane, Figure 1E, Δh) and is also capable of detecting movement
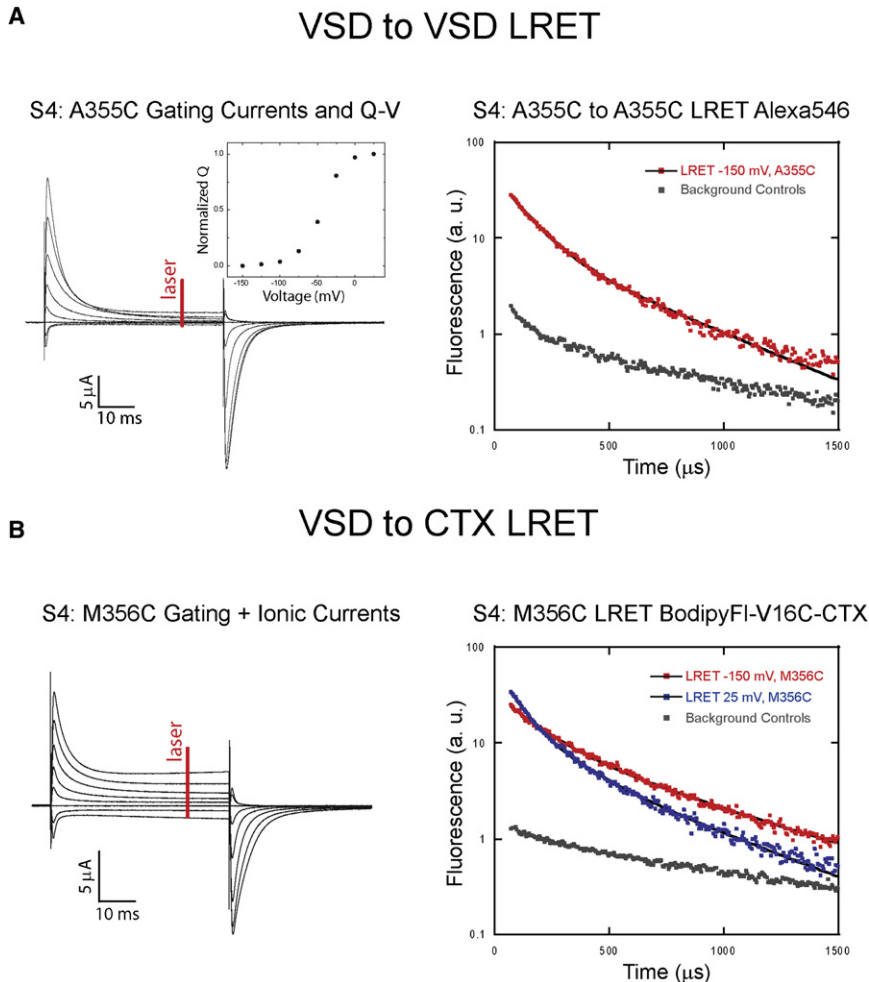
A

VSD to VSD LRET

S4: A355C Gating Currents and Q-V

S4: A355C to A355C LRET Alexa546

Legend:
- LRET −150 mV, A355C
- Background Controls

B

VSD to CTX LRET

S4: M356C Gating + Ionic Currents

S4: M356C LRET BodipyFl-V16C-CTX

Legend:
- LRET −150 mV, M356C
- LRET 25 mV, M356C
- Background Controls

Figure 2. Voltage Clamp and LRET Recordings

(A) VSD to VSD LRET data. (Left) Gating currents for A355C elicited from voltage steps from −100 mV to test voltages ranging from −150 mV to 25 mV. The red line indicates when the laser fires for LRET acquisition. The inset is the normalized charge-voltage (Q-V) curve obtained by integration of the off-gating currents. (Right) LRET signal (red) obtained at −150 mV. Channels were labeled with 4:1 Tb-DTPA-cs124-EMPH:Alexa Fluor 546. The best fit with two exponentials is shown as a black line (τ_1 = 115.6 μs, Rsc = 35.9 Å; and τ_2 = 443.0 μs, Rsa = 46.9 Å). The average signal from four labeled, minus-cysteine control oocytes is shown in gray.

(B) VSD to CTX LRET data. (Left) Gating and ionic currents for M356C elicited from the same pulses as [A]). (Right) LRET signals at −150 mV (red) and 25 mV (blue) are plotted with control signals (gray). Channels were labeled with Tb donors and blocked with 150 nM BodipyFl-V16C-CTX acceptors. The fit to four model-constrained exponentials (see Experimental Procedures) are shown as black lines, and the resulting pyramid edge distances were d_1 = 27 Å, d_2 = d_3 = 34.4 Å, d_4 = 40.5 Å, and d_1 = 23.6 Å, d_2 = 27.1, d_3 = 32.6 Å, d_4 = 35.2 Å.

Shaker (Bezanilla and Stefani, 1998; Stefani et al., 1994). Oocytes expressing Shaker without the A355C mutation were labeled identically and tested for background (Figure 2A, right, gray signal). The signal was fit to two exponentials that were interpreted as distances

tangential to the channel symmetry axis (Figure 1E, Δθ), due to the asymmetrically placed acceptor (Figure 1E, ρ). We have applied both approaches to 19 sites near the transmembrane region of S1–S4 and analyzed the results using a geometric model in which the VSD probe locations lie at the base of an oblique square pyramid with the apex defined by the location of the off-axis acceptor-CTX probe (Figure 1E).

VSD to VSD LRET Measurements

LRET measurements were made after labeling channels with excess donor (four donors:one acceptor) such that a large majority of donor probes have no more than one acceptor (Cha et al., 1999). Multiple donors transfer energy to a single acceptor (Figure 1C). Example data are shown in Figure 2, right, corresponding to LRET trace between Tb-donor-A355C and Alexa Fluor 546-A355C. LRET measurements were acquired 40 ms after initiation of 50 ms test-voltage pulses following 50 ms prepulses to −100 mV (in order to exit inactivation). Between pulses, a holding potential of −80 mV was used. Example gating currents for the S4 to S4 experiment using A355C are shown (Figure 2A, left) with ionic current completely blocked by 2 μM nonfluorescent, wild-type CTX. Integration of the gating currents resulted in the characteristic charge-voltage relation (Figure 2A, inset) for

Rsc and Rsa (Figure 1C). Measured Rsc distances at resting voltage (−150 mV) and activated voltage (25 mV) are tabulated for all sites in Figure 3A. The change in Rsc is small, ranging from −1.5 Å to 1.4 Å. Therefore, LRET does not detect large conformational changes in the radial direction relative to the channel symmetry axis.

VSD to CTX LRET Measurements

Example voltage-clamp recordings for a Tb-donor-M356C to BodipyFl-V16C-CTX acceptor experiment are shown in Figure 2B, left. The amount of toxin is kept low to minimize nonspecific LRET background. CTX (100–150 nM) resulted in near complete ionic current block (Figure 2B) with minimal residual current (almost always less than 20 μA). VSD to CTX LRET signals are shown in Figure 2B, right. Four donor-acceptor distances (d_1, d_2, d_3, and d_4) were estimated with a constrained four-exponential fit, modeled with the pyramid geometry in Figure 1E. The fit function only requires four parameters in order to satisfy two essential assumptions: (1) the donor probes lie on the corners of a square, reducing the number of independent distances to three ($d_4^2 = d_3^2 + d_2^2 - d_1^2$), and (2) all four donor-acceptor distances are equally populated, and therefore, the relative amplitudes are completely determined by the rates of energy transfer
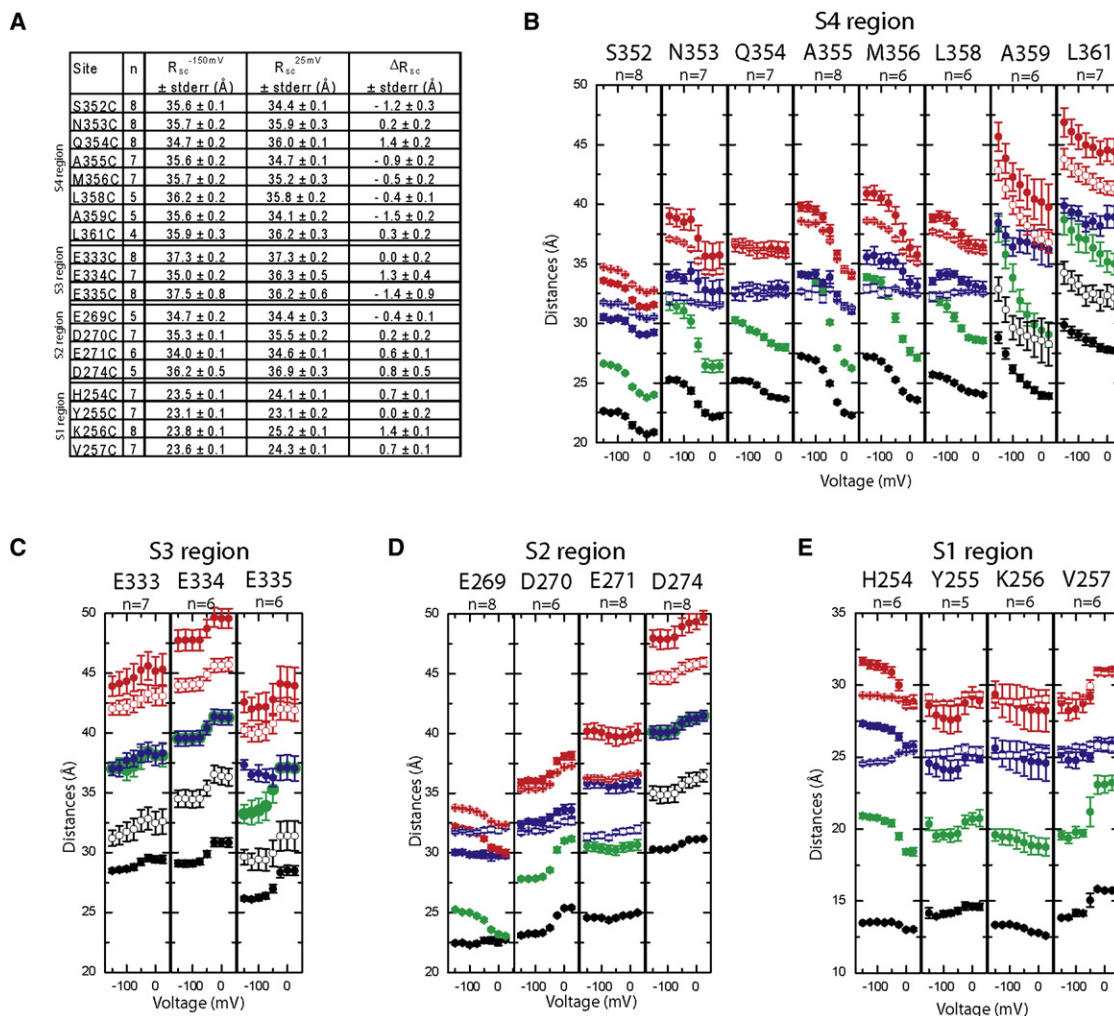
Figure 3. LRET Measured Distances

(A) VSD to VSD LRET distances summary. Tabulated Rsc values for resting VSDs (−150 mV), activated VSDs (25 mV), and the change. Mean and SEM are calculated from n measurements.

(B–E) VSD to CTX distances summary. Pyramid edge distances d_1 (black), d_2 (green), d_3 (blue), and d_4 (red) are plotted as a function of voltage for every experiment. Error bars represent the standard error of the mean for the indicated number of experiments at the top of each graph, n. Closed symbols are for the fitted distance values, and open symbols are for adjusted distances that constrain the acceptor position (see text). In some cases, open and closed symbols overlap.

(see Experimental Procedures). Assumption one is not likely true at intermediate voltage where channel VSDs can be in different conformational states but should be accurate for completely closed and open states. From these results, we calculated the mean distance, d_{mean}, which agreed well with our previously reported averaging technique (Posson et al., 2005) using fits to two unconstrained exponentials (data not shown). We used Bodi-pyFl-V16C-CTX (R_o = 39 Å) for experiments on S2–S4 and Atto465-R19C-CTX (R_o = 27 Å) for experiments on S1 due to the short distances in those experiments.

Measured distances d_1, d_2, d_3, and d_4 are plotted as a function of voltage (closed symbols) for all VSD to CTX experiments in Figures 3B–3E. The open symbols are adjusted distances that constrain the acceptor to a constant position across the entire data set (see Experimental Procedures and below). The model defines d_1 (closed black symbols) $< d_2$ (green) $< d_3$ (blue) $< d_4$ (red). Examination of Figure 3B shows that many sites on or near S4 display a significant change in distances corresponding to a movement toward the toxin upon membrane depolarization. Since no change in S4 Rsc distances were observed (Figure 3A), we conclude that these measurements are tracking a vertical displacement of S4 upon activation. However, we also note that for many S4 sites, d_2 and d_3 are closer in value to each other for hyperpolarized potentials and have significantly differing values at depolarized potentials. Such a trend in the data suggests a movement of the helix tangential to the channel symmetry.

The S3 experiments result in consistent, small-distance changes away from the toxin upon channel activation (Figure 3C). We note that these experiments resulted in $d_2 = d_3$. A constrained fit function was used for such cases (see Experimental

Procedures). For S2 and S1 experiments (Figures 3D and 3E), the results are somewhat more varied, and no consistent movement can be immediately discerned.

Pyramid Model Constraints

LRET measurements provided estimates of five geometric distances for the pyramid model (Figure 1E): Rsc, the base dimension of the pyramid, and d_1 to d_4, the four pyramid edges. These experimental values were used to calculate the other geometric parameters: pyramid height (h) and the position of the apex relative to the base (ρ and θ). Changes in h correspond to protein conformational changes in the "vertical" Z axis direction normal to the plane of the bilayer, changes in θ correspond to tangential movements relative to channel symmetry, and ρ characterizes the asymmetric location of the CTX-acceptor (Figure 1E). We defined the position of the toxin-acceptor to be along the x axis and therefore could calculate (x, y, z) donor probe positions. These positions are not unambiguously determined due to the symmetrical equivalence between a donor positioned at an angle of θ or $-\theta$ with respect to the x axis ($-45° < \theta < 45°$). We therefore used reasonable correspondence with the Kv1.2 chimera crystal structure (Long et al., 2007) and a toxin-binding model (Eriksson and Roux, 2002) to reduce this uncertainty. In the models, the tops of S1 and S2 agree with negative θ values, and S3–S4 agree with mostly positive θ values (see below).

Initially, we examined our results without constraining the position of the acceptor, which is expected to be identical for all experiments. We then calculated adjusted values for d_1–d_4 that were geometrically consistent with a constrained acceptor position for all experiments (see Experimental Procedures). Estimated conformational changes were similar using both methods of analysis. These conformational changes are graphed in Figure 4. The total displacement, Δ, at each site was defined as the distance between estimated (x, y, z) donor coordinates at -150 mV and (x, y, z) donor coordinates at 25 mV (Figure 4A). The graph shows that LRET estimates a 10.4 ± 4.8 Å (standard deviation) displacement for the S4 segment. Total displacement for the other helices is significantly smaller. Figure 4B graphs the change in vertical position (Δh) for each experiment. The vertical contribution to the observed S4 LRET change is $-4.8 ± 1.9$ Å (standard deviation). S3 moves in the opposite direction compared to S4, with $\Delta h = 2.3 ± 1.1$ Å (standard deviation). Figure 4C graphs the movements tangential to channel symmetry, $\Delta\theta$. Again, the largest, most consistent change corresponds to the S4 segment, indicating that it moves outward along a tangential angle upon membrane depolarization.

The calculated change in acceptor position for each experiment, ρ, is tabulated for voltages -150 mV and 25 mV in Figure 4D. The position of the CTX-acceptor probe does not move as a function of voltage, shown as a very small change in ρ, $\Delta\rho = -0.5 ± 1.0$ Å (standard deviation, n = 19) for all experimental sites. For S1 sites using the Atto465-R19C-CTX, $\rho = 10.5 ± 1.2$ Å (standard deviation, n = 32). However, we arrived at variable values for ρ from experiment to experiment on S2–S4 using BodipyFl-V16C-CTX. For one group of experiments (S4, 352–358; S2, 269–270) $\rho = 7.5 ± 1.7$ Å (standard deviation, n = 64; eight voltages for eight experimental sites). A different set of experiments (S4, 359–361; S3, 333–335; S2, 271–274) resulted in higher asymmetry, with $\rho = 12.1 ± 1.4$ Å (standard deviation,

n = 56; eight voltages for seven experimental sites). These differences arise from the unconstrained nature of the fit with regard to the acceptor position and seem unlikely to reflect differences in toxin attachment for the different mutants. For constraining the acceptor position, ρ was fixed to 7.5 Å for all S2–S4 experiments and 10.5 Å for all S1 experiments (see Experimental Procedures).

DISCUSSION

Probe Positions Relative to the Kv1.2 Chimera Structure

Our geometric model allowed us to estimate probe coordinates (x, y, z) for each experiment and compare them with the recent high-resolution structure of the Kv1.2 chimera, pdb 2R9R (Long et al., 2007). Our starting point was a model structure of agitoxin (AgTX) bound to the Shaker channel, kindly provided by Dr. Benoit Roux (Eriksson and Roux, 2002). The model is placed with the channel symmetry axis along the z axis and rotated so that the C_α of P17-AgTX (homologous to the C_α of V16-CTX [Miller, 1995]) is above the x axis (Figure 1E). We modeled the acceptor position for BodipyFl-V16C-CTX experiments to be 7 Å above the C_α of P17-AgTX in the z direction corresponding to the approximate size of the probe and with x = 7.5 Å, corresponding to the constrained value of ρ. For experiments using Atto465-R19C-CTX, the acceptor position was modeled with the same z axis height but is positioned 10.5 Å from the channel axis along an angle defined by the position of the C_α of D20-AgTX. It must be noted that the acceptor reference point is an idealization. In reality, the acceptor has a flexible linker that allows it to wobble around in all directions. This probably results in systematic underestimations of donor to acceptor-toxin distances within the context of the pyramid model. The model locations of the Tb^{3+} donor probes are calculated using the constrained values of d_1–d_4, R_{sc}, h, θ, and ρ. The Kv1.2 chimera crystal structure is placed over the Shaker model using a least-squares alignment of the TTVGYGD selectivity filter coordinates using the program O (Jones et al., 1991).

Figure 5 illustrates the results of these comparisons between estimated probe positions and the Kv1.2 chimera. Figure 5A shows the probe positions from above for the open-state measurements (left) and the closed state (middle). The S1–S4 probe positions are spread apart in the open state. In the closed state, the tangential movement of S4 carries its probe positions closer to the positions of the S2–S3 probes. Figures 5B–5E show S1–S4 probes from above (left) and from the side (middle). Distances between Tb^{3+} donor positions at 25 mV and α carbons for sites in the open-state chimera structure homologous to the labeling sites are tabulated (Figure 5, right).

The probe positions are expected to be in the vicinity of the Shaker protein backbone but separated by distances that are consistent with the structure of the Tb-chelate plus linker. Figure 5A (right) shows a structural model of the Tb-chelate based mostly on a crystal structure (Purdy et al., 2002) with manual modification of the linker attachment to cysteine thiol in order to represent the precise probe molecule used in this study. In this model, the Tb^{3+} to C_α distance is 12.8 Å. Distances between estimated S4 probe locations and Kv1.2 crystal structure coordinates (Figure 5B, right) agree best with the chelate model structure. Most probe positions for S1–S3 experiments are
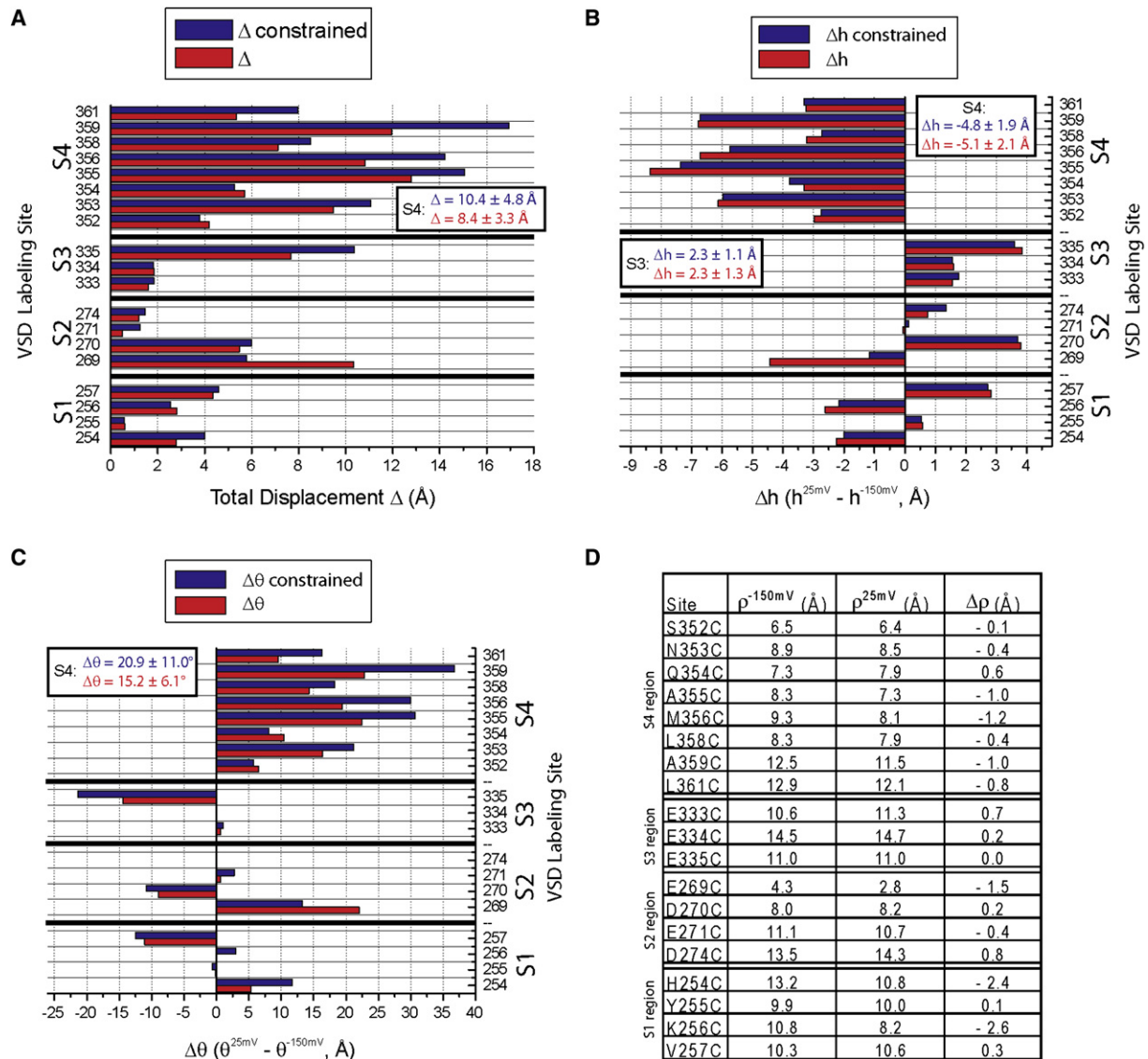
Figure 4. Conformational Changes from Data with (Blue) and without (Red) Constrained Acceptor Positions (See Text)

(A) Total displacement Δ for each VSD site calculated as the distance between estimated (x, y, z) donor probe coordinates at hyperpolarized potential (-150 mV) and depolarized potential (25 mV). The mean displacement of all S4 sites is shown with standard deviation.

(B) Calculated changes in z axis height (Δh) for each site representing the conformational change perpendicular to the membrane. The mean vertical movements for S3 and S4 are shown with standard deviations.

(C) Changes in angular position ($\Delta\theta$) for each site representing the movement tangential to the channel symmetry axis. The mean value for S4 is shown with standard deviation.

(D) Unconstrained values of toxin-acceptor position along the x axis, ρ, for all sites at -150 mV and 25 mV are tabulated and show little voltage dependence.

significantly farther away from their homologous labeling sites in the structure (Figures 5C–5E, right). These discrepancies may result from a number of factors. (1) Probe locations are not quantitatively rigorous due to an imperfect model with systematic errors including the size and mobility of the acceptor probe. (2) Most experiments are from sites on the linker regions that are not conserved between different channels and could have inherent flexibility. (3) Protein dynamics has been shown to affect the closest approach distance between donor and acceptor during

LRET (Chakrabarty et al., 2002), and here, dynamics may "carry" the donor probes closer to the pore domain during the timescale of the measurement ($\sim$100 μs). This is because of the R^{-6} dependence on energy transfer during the *donor's* (submillisecond) lifetime. So, for example, if the donor and/or acceptor sampled *isotropically* the space available to it because of finite linker length during the donor's lifetime, the measured distance would be very close to the distance of closest approach. This last possibility may explain the observation of very similar Rsc values for
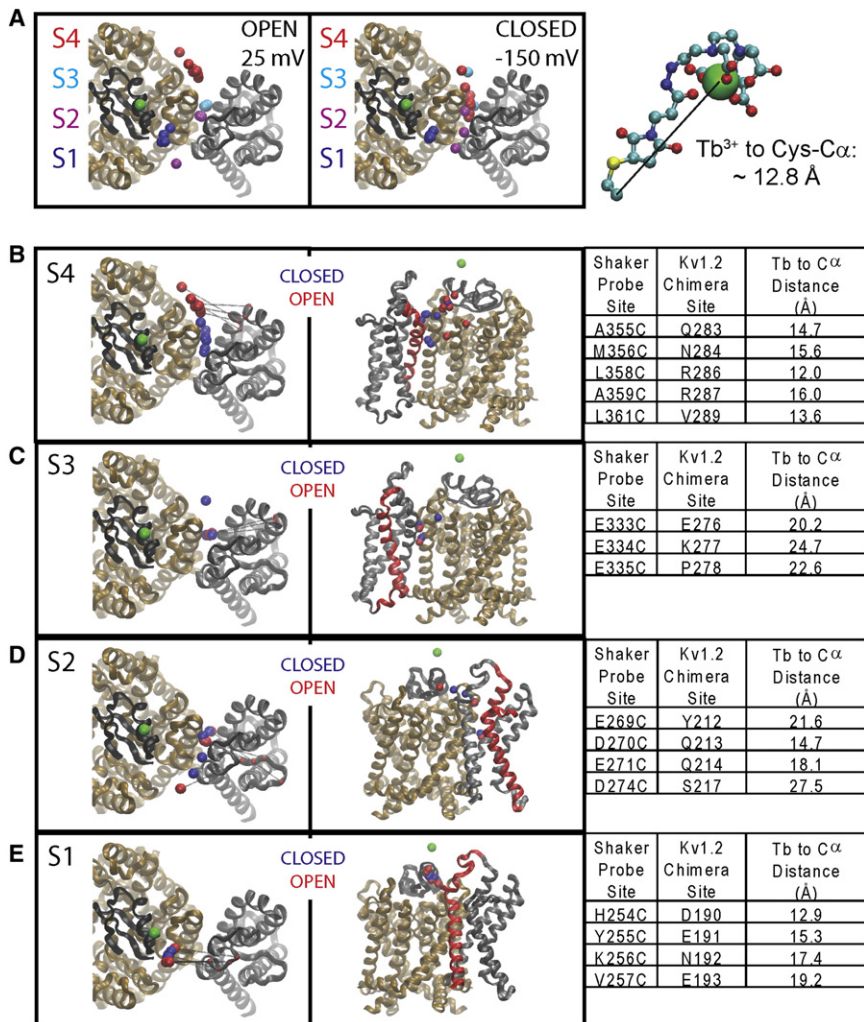
Figure 5. Calculated Probe Positions and Kv1.2 Chimera Structure

(A) Probe positions for S1–S4 (colored spheres) viewed from the extracellular side in the activated state (left) and the closed state (middle). The channel pore domain is colored brown, and a single VSD is gray. The position of the BodipyFl-V16C-CTX acceptor is indicated as a green sphere above the toxin model (black ribbon). Attached chelate probes are red (S4 sites), blue (S3), magenta (S2), and purple (S1). Model structure of the lanthanide chelate probe attached to a cysteine thiol (right). Most of the model is from a recent crystal structure (Purdy et al., 2002), with only the linker modified to reflect the probe used here. The Tb^{3+} to cysteine-C_α distance can be as large as ~12.8 Å.

(B–E) Probe positions for S4–S1 separately viewed from the extracellular side (left) and from the side (middle) for both resting (blue spheres) and activated (red spheres) states. Black lines measure the distance from probe positions at 25 mV to the homologous labeled residue ($C\alpha$) on the crystal structure (left). These distances are tabulated (right). The protein is colored as in (A) except for the middle panel, where the VSD helix of interest is red.

preting LRET results in highly specific structural terms, such as comparisons with a static crystal structure. The purpose of such comparisons is to assist in the visual interpretation of observed LRET changes relative to the VSD structure. The calculated probe positions relative to the Kv1.2 chimera are inherently model dependent and should not be considered to follow unambiguously from the LRET measurements. It is important to remember that, in all energy transfer methods, changes in calculated distance are likely more accurate than static distance comparisons (Clegg, 1995; Selvin, 2002).

Movement of the S1–S3 Segments

Our results estimate only small movements for sites near the S1 and S2 segments (Figures 4 and 5). S1 experiments in particular stay clustered in the same location of Figure 5E for both resting
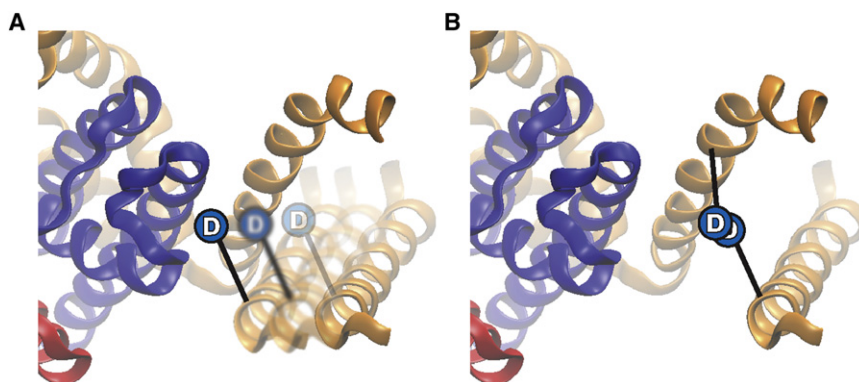
all sites across S2–S4 (Figure 3A), which yields calculated donor positions outlining the pore domain perimeter (Figure 5A). Perhaps lateral mobility of the VSD or individual VSD segments (Figure 6A) allow the closest approach distance to be along this perimeter. Figure 6B illustrates how similar LRET probe positions can be obtained from attachment to completely different protein segments. These issues reflect the difficulty in inter-

Figure 6. Consequences of Probe Linkers and Protein Motion

(A) Protein dynamics may change the effective position measured during LRET. The closest approach distance, pictured against the pore domain, is weighted more heavily than positions farther away.

(B) Probe linker length may produce similar probe positions for very different labeling sites.

and activated VSD conformations. Probes attached to the linker outside of S2 show significant variability in position and no consistent pattern of movement. The experiment at Shaker-S2 D270C shows an almost 4 Å vertical movement in the opposite direction to S4. Such a change might explain the contribution of S2 to the total gating charge (Seoh et al., 1996); however, the data from E269C appear opposite to this proposal. Therefore, these results do not strongly support an important role for significant S1 or S2 movement during voltage sensing. This conclusion is consistent with minimal changes observed in accessibility experiments (Gandhi et al., 2003; Ruta et al., 2005).

It has been proposed that S3 moves with S4 as a rigid body paddle motif (Jiang et al., 2003a, 2003b; Ruta et al., 2005). We observed a consistent change near S3 that indicated a very small vertical movement in the opposite direction from S4 (Figures 4 and 5). This suggests that S3 does not move as a rigid body paddle motif with S4, at least not in the Shaker channel. The absence of significant S3 movement is consistent with studies of Shaker-S3 accessibility using MTS reagents (Gandhi et al., 2003; Gonzalez et al., 2005) and tethered biotin-avidin binding (Darman et al., 2006) but stands in contrast with avidin binding in KvAP (Ruta et al., 2005) and large environmental fluorescence changes on Shaker-S3 (Pathak et al., 2007). It is possible that the large S3–S4 linker in Shaker allows for independent movement of these segments. However, it is known that both S3 and S4 contain critical residues for the interaction between VSDs and gating-modifier toxins (Alabi et al., 2007; Li-Smerin and Swartz, 2000; Swartz, 2007). These toxins bind preferentially to resting voltage sensors but can remain bound during activation, implying limited translocation (Phillips et al., 2005). Therefore, since our measurements show S3 moving opposite to S4, it seems likely that the relative movements of S3 and S4 are important, rather than movements of a rigid body paddle motif.

Movement of the S4 Segment

Here, we show that LRET reports a 10.4 ± 4.8 Å movement for labels attached on and near S4, composed of a vertical displacement of 4.8 ± 1.9 Å, a tangential movement along the channel perimeter of 20.9° ± 11.0° (Figures 4 and 5), and a radial component equal to zero. This movement is significantly larger than our previous estimates from a limited data set and structural assumptions (Posson et al., 2005). A more thorough scan of the S4 region from S352C to L361C revealed variable results, with some residues moving 3–4 Å vertically (S352, Q354, L358, L361), while other sites (N353, A355, M356, A359) moved 6–7 Å vertically. Two sites (S357, I360) did not result in measurable LRET signals, presumably due to labeling inaccessibility. It is possible that the variability in measured probe movement is due to a complicated S4 conformational change such as translation with rotation, a hallmark of helical-screw-type models (Tombola et al., 2006). Recent versions of this model based on the open Kv1.2 crystal structure and new atomic constraints for the resting VSD have estimated the vertical movement of S4 to be ≈ 6.5 Å (Campos et al., 2007) and 6–8 Å (Pathak et al., 2007). These estimations are in good agreement with the larger movements from our data (see Supplemental Data available online).

A second possible explanation for the variability across our S4 data set is that certain sites may be better than others at tracking the underlying movement of S4. Those sites that move into a constrained environment may force rearrangements of the probes relative to the protein during conformational changes. Figure 7A illustrates this in cartoon form, with a donor probe on one side of S4 limited in its movement due the surrounding protein forming an impasse (and so moving just 3 Å, for example). The probe on the opposite side of S4, however, encounters no such obstacle and is free to "follow" the underlying movement of the voltage sensor (and therefore able to move 7 Å, for example).

It has become clear that the S4 charges pass through a proteinaceous, permeation-type pathway referred to as "gating pores" (Tombola et al., 2006). Various mutations at the S4 sites moving through these pores induce voltage-dependent permeation or transport of protons (Starace et al., 1997; Starace and Bezanilla, 2001, 2004), cationic conductance (Tombola et al., 2005, 2007), or disease (Sokolov et al., 2007). It is possible that the movement of our probes might be restricted in the vicinity of the gating pores such that LRET experiments close to the gating charges show limited changes. We mapped our vertical movements onto a helical wheel representation of S4 (Figure 7B). Interestingly, the smaller changes are on the helical face shared by the first three arginine gating charges (R362, R365, R368), whereas the larger changes are on the opposite face. This trend could be explained by S4 rotation, such that as the S4 charges rotate into their gating pore the probes on the same helical face are excluded, inducing probe rearrangement relative to S4. Thus, our data may be consistent with an ~180° rotation; however, our results cannot argue strongly for or against an S4 rotation. The Kv1.2 chimera S4 structure is partly α helical and partly 3_{10} helical, leading MacKinnon and coworkers to suggest the possible importance of conversion between helical types in the voltage-sensing mechanism (Long et al., 2007). This fascinating proposal may allow for internal VSD constraints to be satisfied without requiring complete rotation of the entire S4 helix. Nevertheless, if our smaller vertical movements do represent probe locations that are hindered in their movement, then the remaining LRET measurements would imply an S4 vertical movement on the order of 6–7 Å.

It is well known that the first four arginines on the Shaker S4 (referred to as R1–R4) account for most of the gating charge of ~13 e_0 associated with channel opening (Aggarwal and MacKinnon, 1996; Schoppa et al., 1992; Seoh et al., 1996). Each S4 is predicted to contribute approximately three charges moving across the entire electric field. Evidence presented above favors a short gating pore that focuses the electric field over a narrow region within the VSD. If the gap between external and internal electrical environments is very thin, on the order of a few angstroms (Ahern and Horn, 2005), the vertical S4 displacement will likely need to traverse the distance between three arginine gating charges in order to account for the total gating charge. In the Kv1.2 chimera structure, the z axis distance between C_αs from the Shaker R1 position (Q290 in the chimera) to R3 (chimera R296) is 8.1 Å. A similar measurement between C_αs from R2 (chimera R293) to R4 (chimera R299) yields 10.0 Å. Vertical displacements somewhat smaller in magnitude are able to account for the total gating charge of the channel (Chanda et al., 2005), especially when considering the length and flexibility of arginine side chains. Therefore, the LRET estimated
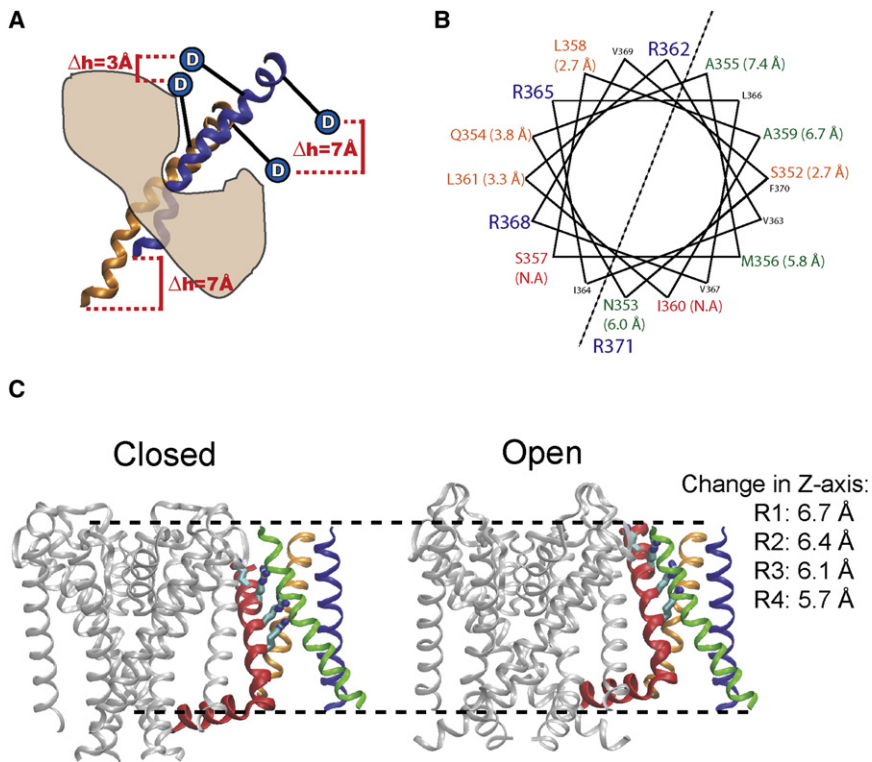
Figure 7. Interpretation of S4 Data Set

(A) Possible rationale for variable results between S4 experiments. The S4 carries gating charges through "gating pores," which may restrict the movement of LRET probes attached to specific positions. Here, S4 is shown moving 7 Å vertically through a gating pathway. The donor probe on the right is unconstrained by neighboring protein elements and changes its vertical position by 7 Å. The probe on the left encounters an obstacle and is forced to reorient relative to S4, resulting in a vertical position change of only 3 Å.

(B) Helical wheel representation of S4 sites studied with LRET. Sites that resulted in a vertical displacement >5 Å are shown in green, <5 Å are orange, and sites not accessible to labeling (NA) are red. Vertical displacements are indicated in parentheses. Arginine gating charges are blue. A dashed line separates the two distinct groups of data. The side of S4 containing the gating charges showed only ~3 Å movement, whereas the opposite face showed ~6–7 Å movement.

(C) A simple model illustrating the vertical movement of S4 between closed and open states is shown. The pore domains are gray, S1 is green, S2 is blue, S3 is orange, and S4 is red. The closed model (left) is made using the pore domain from MloK1 (pdb code 3BEH) with S1–S4 and the S4–S5 linker taken from the Kv1.2 chimera structure (pdb code 2R9R). The S1–S3 are placed according to alignment between the channel selectivity filters, the S4 and S4–S5 linker are placed according to an alignment with the S4–S5 linker of MloK1. The open-state model (right) is simply the Kv1.2 crystal structure. S1–S2 and S3–S4 linkers have been removed for clarity, and residues corresponding to Shaker gating charges are detailed. Dashed lines indicate the extent of S4 z axis movement and vertical changes for α carbons corresponding to gating charge positions, R1–R4, are ~6–6.5 Å.

conformational changes reported here are consistent with the large VSD gating charge moving across a short gating pathway.

Bezanilla and coworkers found disulphide crosslinks in the resting VSD between S4 (site R1) and the S1 segment at I124 (Kv1.2 chimera, I177) and S2 at I287 (Kv1.2 chimera, I230) (Campos et al., 2007). In the crystal structure, the corresponding C_αs between these sites are 8.6 Å and 10.4 Å apart along the z axis, respectively. Our measurements do not rule out the possibility that S2 moves "up" slightly during hyperpolarization, which would reduce the distance S4 needs to traverse toward I287 in the closed conformation. The direction and magnitude of S4 movement in our study agree well with a conformational change that satisfies these crosslinks in the resting VSD and moves to the depolarized position of the crystal structure. Our measurements do not seem to agree, however, with a recent model based on constraints found for the hyperpolarization-activated KAT1 (see Supplemental Data) channel (Grabe et al., 2007), potentially due to difficulty in mapping the results onto Shaker (Pathak et al., 2007).

Recently, a high-resolution structure of the six-transmembrane-helix domain from a bacterial CNG channel, MloK1 from *Mesorhizobium loti* (Nimigean et al., 2004), has been solved (Clayton et al., 2008). This structure contains an S1–S4 domain that likely does not sense voltage, due to the absence of arginines at the corresponding gating charge locations in Kv channels. However, as discussed by Morais-Cabral and coworkers, the pore domain in the new structure adopts a closed conforma-

tion, and so the relative position of the S4–S5 linker in this state can be examined. We placed the Kv1.2 chimera VSD structure around the closed MloK1 pore domain using structural alignment of the selectivity filter coordinates. We then moved S4 and the S4–S5 linker using structural alignment with the MloK1 S4–S5 linker for a simple model of a closed Kv channel VSD (Figure 7C, left). For comparison, the Kv1.2 chimera crystal structure is shown in Figure 7C, right. Horizontal dashed lines indicate the extent of S4 vertical movement between the models. The measured change in z axis height for α carbons corresponding to gating charge residues is ~6–6.5 Å, in agreement with the LRET estimation. The simple model of S4 motion in Figure 7 does not attempt to precisely illustrate atomic detail. In particular, S1–S3 remain static between closed and open, no rotations (Campos et al., 2007; Pathak et al., 2007), or secondary-structure changes (Long et al., 2007) of the S4 segment are imposed to satisfy internal VSD constraints, no reorientations of the gating charges are invoked, and the S4 and S4–S5 linker are assumed to move as a rigid body. For a comparison of this simple S4 closed-state model and the recent models of Yarov-Yarovoy and coworkers (Pathak et al., 2007) and Grabe and coworkers (Grabe et al., 2007), see Supplemental Data.

Therefore, the present LRET results represent an independent and self-contained measure of voltage-sensor movement that are consistent with a number of important but less direct measures of conformational movements: available structural data

for six-transmembrane domain channels, available atomic constraints within the voltage-sensing domain, and the necessity to account for channel gating charge. The S4 segment translates ~10 Å with a vertical component as large as ~6–7 Å. The S3 segment, rather than moving with S4 as a paddle motif, is probably critical for stabilizing the aqueous crevices and lipid bilayer environment around S4.

EXPERIMENTAL PROCEDURES

Toxin Biochemistry, Shaker Expression, and Labeling

R19C-CTX was prepared, labeled with Atto465-maleimide dye (Atto-Tec), and purified as described previously (Shimony et al., 1994). V16C-CTX was prepared and labeled with BodipyFl-maleimide (Invitrogen) by a modified procedure. Briefly, purified gene9-CTX fusion protein was labeled prior to proteolytic cleavage and CTX-N terminus cyclization. Unreacted dye was removed by gel filtration (Pierce). The toxin was further purified by binding to cation-exchange sephadex (Sigma), washed, and eluted with high salt. Mass spectrometry verified the theoretical mass for labeled toxin, and no HPLC purification was employed. High-affinity binding to Shaker for both toxin preparations was verified qualitatively by observation of slow toxin wash-off (τ ~hours). For one control experiment, the measured LRET signal was observed to persist on a similar timescale during toxin wash-off (data not shown).

The Shaker construct was the fast inactivation-removed, Shaker H4IR, with background mutations F425G, K427D that increase toxin binding to subnanomolar affinity (Goldstein et al., 1994). Single cysteine mutations were introduced using the QuikChange kit (Stratagene) and verified by sequencing. mRNA transcripts were produced with the mMessage mMachine T7 Ultra kit (Ambion), and 20 ng quantities were injected into *Xenopus* oocytes. Surface expression of the channels was inhibited for 2–3 days by incubation at 12°C in 60% L15 media (Invitrogen) plus 500 μM dithiothreitol (DTT), after which DTT was washed away and background cysteines on the plasma membrane were blocked by 1 hr labeling with 500 μM β-maleimido-propionic acid (Sigma). Preblocked oocytes were then placed at 18°C for 18–30 hr in L15 plus 25 μM DTT to allow trafficking of channels to the membrane (Mannuzzu et al., 1996). Prior to thiol modification, probes were placed in depolarizing solution (in mM: 120 K-MES, 2 CaCl₂, 1 MgCl₂, 10 HEPES [pH 7.5]) plus 100 μM DTT for 30 min, after which DTT was removed.

For VSD to VSD LRET experiments, cells were transferred to depolarizing solution plus 4:1 donor to acceptor ratio (Cha et al., 1999); 80 μM Tb-DTPA-cs124-EMPH (Chen and Selvin, 1999), 20 μM Alexa Fluor 546-maleimide (Invitrogen) for 30 min. Cells were washed and experiments were performed in bath (in mM: 120 N-methyl D-glucamine, 2 Ca-MES, 10 HEPES [pH 7.8]) plus 2 μM wild-type CTX (Alomone Labs) for saturated channel block.

For VSD to CTX LRET experiments, cells were labeled in depolarizing solution plus 80 μM Tb-DTPA-cs124-EMPH for 30 min. Experiments were performed in bath plus 100–150 nM fluorescent CTX for nearly complete block of channels. Residual current was normally limited to around 20 μA or less and was never higher than 40 μA to insure accurate voltage clamping (Baumgartner et al., 1999).

LRET Apparatus and Distance Determination

The apparatus has been previously described (Posson et al., 2005). Briefly, oocytes are clamped with a CA-1B two-electrode voltage clamp (Dagan) over a 40× quartz objective (Partec). 337 nm, N₂-laser excitation pulses are triggered 40 ms into 50 ms voltage-clamping test pulses. The fluorescence signal is averaged over ten laser pulses (taken at 1 Hz) for acceptable fluorescence signal/noise. Fluorescence emission is collected through D490/10, HQ520/20, and HQ570/10 for Tb-DTPA, BodipyFl/Atto465, and Alexa 546, respectively, and recorded with photomultiplier tubes (R943-02, Hamamatsu) that were electronically gated-on (Products for Research) after the laser pulse with a measurement dead-time of 70 μs.

VSD to VSD LRET sensitized acceptor emission was fit with two exponentials (four parameters: A_1, τ_1, A_2, τ_2), $A_1 \exp(-t/\tau_1) + A_2 \exp(-t/\tau_2)$. Distances Rsc (subunits contiguous) and Rsa (subunits across) were calculated from τ_1

and τ_2. For all S2–S4 measurements, Rsa/Rsc = 1.31 ± 0.04 (standard deviation, n = 784), and for S1 the Rsc component was too fast to determine. These results deviate slightly from the Pythagorean theorem for which Rsa/Rsc = 1.41. For S2–S4, we assumed that Rsc was determined at higher accuracy due to the ~8-fold greater predicted amplitude corresponding to Rsc. R_o for Tb to Alexa 546 was determined to be 55 Å.

VSD to CTX LRET sensitized acceptor emission were fit with a four-exponential model (four parameters: A, d_1, d_2, d_3) that followed from three assumptions: (1) the results correspond geometrically with an oblique, square pyramid (Figure 1E) resulting in only three independent donor-acceptor distances d_1–d_3, with d_4 given by $d_4^2 = d_3^2 + d_2^2 - d_1^2$ ($d_4 > d_3 > d_2 > d_1$); (2) the four donor-acceptor distances are equally populated and therefore relative amplitudes between components are determined by the rates of energy transfer (Heyduk and Heyduk, 2001); and (3) the minor component from the biexponential donor (75% 1600 μs, 25% 300 μs) can be ignored (Posson et al., 2005). The fit function was of the form A $[k_1 \exp(-t/\tau_1) + k_2 \exp(-t/\tau_2) + k_3 \exp(-t/\tau_3) + k_4 \exp(-t/\tau_4)]$, where $\tau_n = \tau_D(d_n^6/(d_n^6 + R_o^6))$ and $k_n = 1/\tau_n - 1/\tau_D$. The donor lifetime, τ_D, was 1600 μs. R_o was determined to be 39 Å for Tb to BodipyFl and 27 Å for Tb³⁺ to Atto465. In cases where the fit tried to converge to a solution with $d_2 = d_3$, a three-parameter version was used constraining $d_2 = d_3$. The geometric parameters (Figure 1E) h, ρ, and θ were calculated from d_1–d_4 and Rsc. We fit the data into a model with constrained acceptor positions with $\rho = 7.5$ Å for BodipyFl-V16C-CTX experiments and $\rho = 10.5$ Å for Atto465-R19C-CTX experiments. We reasoned that d_1 and d_2 were likely of higher accuracy than d_3 and d_4 due to the larger amplitudes of these components. We calculated new values of d_3 and d_4 (open symbols in Figures 3B–3E) that are geometrically consistent with the fixed values of the acceptor position and the measured values of d_1, d_2, and Rsc. For experiments that yielded large values for ρ, the above procedure was not possible. d_2 and d_3 were accepted, and new values for d_1 and d_4 were calculated for geometric consistency. Simulated data designed to test the accuracy of the VSD to CTX fitting model are presented in the Supplemental Data. From ten data simulations, 40 distances were determined with an average error (percent difference from theoretical) of 3.9% ± 2.3% (standard deviation).

SUPPLEMENTAL DATA

ACKNOWLEDGMENTS

REFERENCES

Aggarwal, S.K., and MacKinnon, R. (1996). Contribution of the S4 segment to gating charge in the Shaker K+ channel. Neuron *16*, 1169–1177.

Ahern, C.A., and Horn, R. (2004). Stirring up controversy with a voltage sensor paddle. Trends Neurosci. *27*, 303–307.

Ahern, C.A., and Horn, R. (2005). Focused electric field across the voltage sensor of potassium channels. Neuron *48*, 25–29.

Alabi, A.A., Bahamonde, M.I., Jung, H.J., Kim, J.I., and Swartz, K.J. (2007). Portability of paddle motif function and pharmacology in voltage sensors. Nature *450*, 370–375.

Baumgartner, W., Islas, L., and Sigworth, F.J. (1999). Two-microelectrode voltage clamp of Xenopus oocytes: voltage errors and compensation for local current flow. Biophys. J. *77*, 1980–1991.

Bezanilla, F. (2005). Voltage-gated ion channels. IEEE Trans. Nanobioscience *4*, 34–48.

Bezanilla, F., and Stefani, E. (1998). Gating currents. Methods Enzymol. *293*, 331–352.

Blunck, R., Starace, D.M., Correa, A.M., and Bezanilla, F. (2004). Detecting rearrangements of shaker and NaChBac in real-time with fluorescence spectroscopy in patch-clamped mammalian cells. Biophys. J. *86*, 3966–3980.

Campos, F.V., Chanda, B., Roux, B., and Bezanilla, F. (2007). Two atomic constraints unambiguously position the S4 segment relative to S1 and S2 segments in the closed state of Shaker K channel. Proc. Natl. Acad. Sci. USA *104*, 7904–7909.

Cha, A., and Bezanilla, F. (1997). Characterizing voltage-dependent conformational changes in the *Shaker* K+ channel with fluorescence. Neuron *19*, 1127–1140.

Cha, A., Snyder, G.E., Selvin, P.R., and Bezanilla, F. (1999). Atomic scale movement of the voltage sensing region in a potassium channel measured via spectroscopy. Nature *402*, 809–813.

Chakrabarty, T., Xiao, M., Cooke, R., and Selvin, P.R. (2002). Holding two heads together: Stability of the Myosin II rod measured by resonance energy transfer between the heads. Proc. Natl. Acad. Sci. USA *99*, 6011–6016.

Chanda, B., Asamoah, O.K., and Bezanilla, F. (2004). Coupling interactions between voltage sensors of the sodium channel as revealed by site-specific measurements. J. Gen. Physiol. *123*, 217–230.

Chanda, B., Asamoah, O.K., Blunck, R., Roux, B., and Bezanilla, F. (2005). Gating charge displacement in voltage-gated ion channels involves limited transmembrane movement. Nature *436*, 852–856.

Chen, J., and Selvin, P.R. (1999). Thiol-reactive luminescent lanthanide chelates. Bioconjug. Chem. *10*, 311–315.

Clayton, G.M., Altieri, S., Heginbotham, L., Unger, V.M., and Morais-Cabral, J.H. (2008). Structure of the transmembrane regions of a bacterial cyclic nucleotide-regulated channel. Proc. Natl. Acad. Sci. USA *105*, 1511–1515.

Clegg, R.M. (1995). Fluorescence resonance energy transfer. Curr. Opin. Biotechnol. *6*, 103–110.

Darman, R.B., Ivy, A.A., Ketty, V., and Blaustein, R.O. (2006). Constraints on voltage sensor movement in the shaker K+ channel. J. Gen. Physiol. *128*, 687–699.

Eriksson, M.A., and Roux, B. (2002). Modeling the structure of agitoxin in complex with the Shaker K+ channel: a computational approach based on experimental distance restraints extracted from thermodynamic mutant cycles. Biophys. J. *83*, 2595–2609.

Gandhi, C.S., Clark, E., Loots, E., Pralle, A., and Isacoff, E.Y. (2003). The orientation and molecular movement of a k(+) channel voltage-sensing domain. Neuron *40*, 515–525.

Glauner, K.S., Mannuzzu, L.M., Gandhi, C.S., and Isacoff, E.Y. (1999). Spectroscopic mapping of voltage sensor movement in the Shaker potassium channel. Nature *402*, 813–817.

Goldstein, S.A., Pheasant, D.J., and Miller, C. (1994). The charybdotoxin receptor of a Shaker K+ channel: peptide and channel residues mediating molecular recognition. Neuron *12*, 1377–1388.

Gonzalez, C., Morera, F.J., Rosenmann, E., Alvarez, O., and Latorre, R. (2005). S3b amino acid residues do not shuttle across the bilayer in voltage-dependent Shaker K+ channels. Proc. Natl. Acad. Sci. USA *102*, 5020–5025.

Grabe, M., Lai, H.C., Jain, M., Jan, Y.N., and Jan, L.Y. (2007). Structure prediction for the down state of a potassium channel voltage sensor. Nature *445*, 550–553.

Heyduk, T., and Heyduk, E. (2001). Luminescence energy transfer with lanthanide chelates: interpretation of sensitized acceptor decay amplitudes. Anal. Biochem. *289*, 60–67.

Hille, B. (2001). Ion Channels of Excitable Membranes, Third Edition (Sunderland, MA: Sinauer).

Hodgkin, A.L., and Huxley, A.F. (1952). A quantitative description of membrane current and its application to conduction and excitation in nerve. J. Physiol. *117*, 500–544.

Jiang, Y., Lee, A., Chen, J., Ruta, V., Cadene, M., Chait, B.T., and MacKinnon, R. (2003a). X-ray structure of a voltage-dependent K+ channel. Nature *423*, 33–41.

Jiang, Y., Ruta, V., Chen, J., Lee, A., and MacKinnon, R. (2003b). The principle of gating charge movement in a voltage-dependent K+ channel. Nature *423*, 42–48.

Jones, T.A., Zou, J.Y., Cowan, S.W., and Kjeldgaard, M. (1991). Improved methods for building protein models in electron density maps and the location of errors in these models. Acta Crystallogr. A *47*, 110–119.

Kumanovics, A., Levin, G., and Blount, P. (2002). Family ties of gated pores: evolution of the sensor module. FASEB J. *16*, 1623–1629.

Lee, S.Y., Lee, A., Chen, J., and Mackinnon, R. (2005). Structure of the KvAP voltage-dependent K+ channel and its dependence on the lipid membrane. Proc. Natl. Acad. Sci. USA *102*, 15441–15446.

Li-Smerin, Y., and Swartz, K.J. (2000). Localization and molecular determinants of the Hanatoxin receptors on the voltage-sensing domains of a K(+) channel. J. Gen. Physiol. *115*, 673–684.

Long, S.B., Campbell, E.B., and Mackinnon, R. (2005). Crystal structure of a mammalian voltage-dependent Shaker family K+ channel. Science *309*, 897–903.

Long, S.B., Tao, X., Campbell, E.B., and MacKinnon, R. (2007). Atomic structure of a voltage-dependent K+ channel in a lipid membrane-like environment. Nature *450*, 376–382.

Mannuzzu, L.M., Moronne, M.M., and Isacoff, E.Y. (1996). Direct physical measure of conformational rearrangement underlying potassium channel gating. Science *271*, 213–216.

Miller, C. (1995). The charybdotoxin family of K+ channel-blocking peptides. Neuron *15*, 5–10.

Murata, Y., Iwasaki, H., Sasaki, M., Inaba, K., and Okamura, Y. (2005). Phosphoinositide phosphatase activity coupled to an intrinsic voltage sensor. Nature *435*, 1239–1243.

Nimigean, C.M., Shane, T., and Miller, C. (2004). A cyclic nucleotide modulated prokaryotic K+ channel. J. Gen. Physiol. *124*, 203–210.

Pathak, M., Kurtz, L., Tombola, F., and Isacoff, E. (2005). The cooperative voltage sensor motion that gates a potassium channel. J. Gen. Physiol. *125*, 57–69.

Pathak, M.M., Yarov-Yarovoy, V., Agarwal, G., Roux, B., Barth, P., Kohout, S., Tombola, F., and Isacoff, E.Y. (2007). Closing in on the resting state of the Shaker K(+) channel. Neuron *56*, 124–140.

Phillips, L.R., Milescu, M., Li-Smerin, Y., Mindell, J.A., Kim, J.I., and Swartz, K.J. (2005). Voltage-sensor activation with a tarantula toxin as cargo. Nature *436*, 857–860.

Posson, D.J., Ge, P., Miller, C., Bezanilla, F., and Selvin, P.R. (2005). Small vertical movement of a K+ channel voltage sensor measured with luminescence energy transfer. Nature *436*, 848–851.

Purdy, M.D., Ge, P., Chen, J., Selvin, P.R., and Wiener, M.C. (2002). Thiol-reactive lanthanide chelates for phasing protein x-ray diffraction data. Acta Crystallogr. D Biol. Crystallogr. *58*, 1111–1117.

Reifenberger, J.G., Snyder, G.E., Baym, G., and Selvin, P.R. (2003). Emission polarization of europium and terbium chelates. J. Phys. Chem. B *107*, 12862–12873.

Richardson, J., Blunck, R., Ge, P., Selvin, P.R., Bezanilla, F., Papazian, D.M., and Correa, A.M. (2006). Distance measurements reveal a common topology

of prokaryotic voltage-gated ion channels in the lipid bilayer. Proc. Natl. Acad. Sci. USA *103*, 15865–15870.

Ruta, V., Chen, J., and MacKinnon, R. (2005). Calibrated measurement of gating-charge arginine displacement in the KvAP voltage-dependent K+ channel. Cell *123*, 463–475.

Sasaki, M., Takagi, M., and Okumura, Y. (2006). A voltage sensor-domain protein is a voltage-gated proton channel. Science *312*, 589–592.

Schoppa, N.E., McCormack, K., Tanouye, M.A., and Sigworth, F.J. (1992). The Size of Gating Charge in Wild-Type and Mutant Shaker Potassium Channels. Science *255*, 1712–1715.

Selvin, P.R. (2002). Principles and biophysical applications of luminescent lanthanide probes. Annu. Rev. Biophys. Biomol. Struct. *31*, 275–302.

Seoh, S.-A., Papazian, D.M., Sigg, D., and Bezanilla, F. (1996). Voltage-sensing residues in the S2 and S4 segments of the Shaker K+ channel. Neuron *16*, 1159–1167.

Shimony, E., Sun, T., Kolmakova-Partensky, L., and Miller, C. (1994). Engineering a uniquely reactive thiol into a cysteine-rich peptide. Protein Eng. *7*, 503–507.

Smith, P.L., and Yellen, G. (2002). Fast and slow voltage sensor movements in HERG potassium channels. J. Gen. Physiol. *119*, 275–293.

Sokolov, S., Scheuer, T., and Catterall, W.A. (2007). Gating pore current in an inherited ion channelopathy. Nature *446*, 76–78.

Sonnleitner, A., Mannuzzu, L.M., Terakawa, S., and Isacoff, E.Y. (2002). Structural rearrangements in single ion channels detected optically in living cells. Proc. Natl. Acad. Sci. USA *99*, 12759–12764.

Starace, D.M., and Bezanilla, F. (2001). Histidine scanning mutagenesis of basic residues of the S4 segment of the shaker k+ channel. J. Gen. Physiol. *117*, 469–490.

Starace, D.M., and Bezanilla, F. (2004). A proton pore in a potassium channel voltage sensor reveals a focused electric field. Nature *427*, 548–553.

Starace, D., Stefani, E., and Bezanilla, F. (1997). Voltage-dependent proton transport by the voltage sensor of the Shaker K+ channel. Neuron *19*, 1319–1327.

Stefani, E., Toro, L., Perozo, E., and Bezanilla, F. (1994). Gating of Shaker K+ channels: I. Ionic and gating currents. Biophys. J. *66*, 996–1010.

Stryer, L., and Haugland, R.P. (1967). Energy transfer: a spectroscopic ruler. Proc. Natl. Acad. Sci. USA *58*, 719–726.

Swartz, K.J. (2007). Tarantula toxins interacting with voltage sensors in potassium channels. Toxicon *49*, 213–230.

Tempel, B.L., Papazian, D.M., Schwarz, T.L., Jan, Y.L., and Jan, L.Y. (1987). Sequence of a probable potassium channel component encoded at *Shaker* locus of *Drosophila*. Science *237*, 770–775.

Tombola, F., Pathak, M.M., and Isacoff, E.Y. (2005). Voltage-sensing arginines in a potassium channel permeate and occlude cation-selective pores. Neuron *45*, 379–388.

Tombola, F., Pathak, M.M., and Isacoff, E.Y. (2006). How does voltage open an ion channel? Annu. Rev. Cell Dev. Biol. *22*, 23–52.

Tombola, F., Pathak, M.M., Gorostiza, P., and Isacoff, E.Y. (2007). The twisted ion-permeation pathway of a resting voltage-sensing domain. Nature *445*, 546–549.